UCRL-86158
PREPRINT
CONF-811113--33

MASTER

WAVELENGTH DEPENDENCE AND EFFICIENCY OF LASER HEATING OF DT-FILLED POLYMER-COATED GLASS MICROSPHERES AT CRYOGENIC TEMPERATURES

Dale H. Darling
Thomas P. Bernat
Brent H. Ives

This paper was prepared for submittal to the
28th National American Vacuum Society Symposium
Anaheim, Calif.
November 2-6, 1981

September 24, 1981

Lawrence Livermore Laboratory

WAVELENGTH DEPENDENCE AND EFFICIENCY OF LASER HEATING OF DT-FILLED POLYMER-COATED GLASS MICROSPHERES AT CRYOGENIC TEMPERATURES*

Dale H. Darling, Thomas P. Bernat and Brent H. Ives

LAWRENCE LIVERMORE NATIONAL LABORATORY
P. O. Box 5508
Livermore, CA 94550

ABSTRACT

The utility of using a heating laser to vaporise the solid DT fill in the heat-pulse fast-refreeze method for production of uniform solid DT layers inside polymer coated glass microsphere targets, as well as the susceptibility of such cryogenic targets to driving laser ASE depends critically on the amount of incident laser energy absorbed by the target. The relative absorption efficiency may vary with target material (polymer, glass and solid DT layers) as well as the wavelength of the illuminating laser.

We have determined experimentally the fraction of laser light incident on DT filled cryogenic polymer coated and bare glass microsphere targets that is absorbed to produce target heating. Data has been obtained for bare glass and CH and CF polymer coated microspheres at 488 nm and 632 nm laser wavelengths.

The measurement technique used and experimental results obtained will be presented.

*Work performed under the auspices of the U.S. Department of Energy by the Lawrence Livermore National Laboratory under contract number W-7405-ENG-48.

Introduction

Some direct irradiation cryogenic laser fusion targets consist of polymer coated hollow glass microspheres with the DT fuel frozen out in a thin solid layer on the interior of the target. To insure adequate symmetry during the target implosion, the frozen DT layer must be smooth and highly concentric. Production of such a high quality layer requires that the DT fuel be rapidly frozen from the vapor. To facilitate uniform layer production a laser heat pulse fast refreeze (LHPFR) technique was developed.[1] In the ideal application of the LHPFR technique the heating laser light would be strongly absorbed only by the DT fuel which would be heated and vaporized, while the rest of the target remains unheated. After the laser pulse the gaseous fuel would rapidly and uniformly condense out onto the cold target walls. For polymer coated or bare glass cryogenic targets ideal LHPFR behavior is not expected, in that the bulk of the heating laser energy will be deposited in the polymer and glass layers. Energy transport to the fuel will occur by thermal diffusion resulting in a temperature distribution through the target significantly different than the ideal case.

Absorption of laser light by the non-fuel components of the target can also place a limit on the maximum heating fluence incident on the target, if damage to target components is to be avoided. Such damage could occur through mechanical failure of polymer coatings due to large stresses generated by differential thermal expansion of bonded polymer and glass layers. This failure mode in addition to being relevant when applying the LHPFR technique, may also represent a target failure mechanism due to driver laser Amplified Spontaneous Emission (A.S.E.) power incident prior to the main drive pulse.

In order to model non-ideal LHPFR conditions, and to predict damage thresholds to cryogenic targets, we measured laser power coupling efficiency to cryogenic targets at 632 nm and 400 nm wavelengths. The targets tested were of filled bare glass and polymer coated microspheres. The targets were sandwiched between two 50 nm formvar films which were mounted on a copper washer assembly which facilitated rapid and accurate target placement inside the sample cell. The CF and CH coatings were deposited by a plasma polymerization process. Relevant target parameters are listed in Table I.

TABLE I

Target	ID μm	OD μm	Glass Shell μm	Polymer Shell μm	Fill
RF6	141.4	181.0	4.5	15.5 CF	DT 6mg/cc
RF9	144.2	153	4.4	none	DT -
RF13	200.6	254	6	20.74 CH	DT 10
RF14	143.4	179.6	4	14.1 CF	DT 10

Method of Measurement

The targets tested were enclosed in a copper cell attached to the cold finger of a Helitran refrigerator shown in Fig. 1. This copper sample cell provided a highly isotropic thermal environment. Thermal contact between the target and the sample cell was maintained via helium exchange gas. The degree of thermal coupling could be controlled by varying the exchange gas pressure, when operating in the molecular bombardment regime (i.e. molecular mean free path comparable to target dimension). At higher exchange gas pressures (typically greater than 1000 μm Hg) transport occurs in the thermal conduction regime. In this regime the thermal conductivity is independent of the gas pressure and is solely a function of gas temperature. For helium gas the thermal conductivity is given by

$$K(T) = 3.34 \times 10^{-5}\ T^{0.682}\ \text{watts/cm-K}$$

valid over the temperature range 4K to 300K.

Optical access to the target was through heat absorbing windows in the sample cell and surrounding vacuum chamber. The optical system for visual observation of the target and introduction of the heating laser beam is diagrammed in Fig. 2. The heating laser is incident on the target through the microscope objective that is used to image the target, and is focused prior to reaching the target. The diverging laser beam is incident in a spherical patch on the target as diagrammed in Fig. 3. With this focusing arrangement all of the heating laser power which enters the sample cell is incident on the target. However only a fraction of this incident laser energy is absorbed by and heats the target. Under steady state conditions the laser power absorbed equals the conduction heat flow between the target at some unknown elevated temperature and the chamber at a known controlled temperature. If there is sufficient helium exchange gas in the cell to be in the thermal conduction regime then the heat flow (assuming spherical symmetry and chamber dimensions--large compared to the target sphere) is given in watts by

$$Q = 2.5\times10^{-4}\, R_s \left(T_{wall}^{1.682} - T_{target}^{1.682} \right)$$

where R_s is the external radius of the target in cm, T_{wall} is the chamber wall temperature and T_{target} is the target temperature. To obtain a reproducible and identifiable target temperature fixed point, the heater laser power was incremented until the DT fuel solid-liquid phase transition was observed implying a target temperature of 19.8K. The conduction regime heat flow "Q" is calculated and compared with the measured incident heating laser power required to produce the phase change when operating in the conduction regime. The on-target laser power required to melt the fuel as a function of the helium exchange gas pressure is shown in Figures 4a and 4b for target BF14. In Figures 4a and 4b we have data for 488 nm Ar ion and 632 nm He-Ne heating laser illumination respectively, with two different sample cell temperatures for each wavelength set. The asymptotic approach to some power level at higher pressures indicates conduction regime operation.

Helium exchange gas pressures were measured with a Barotron pressure monitor, and a thermomolecular effect correction was carried out for each pressure reading using a computer generated solution of the Weber-Schmidt equation.(2) The heating laser fluence on target is determined by measuring the power of a fraction of the beam diverted off to a power meter and applying an experimentally determined correction factor to account for losses in the optical chain. Sample cell temperature was measured using a calibrated silicon diode thermometer accurate to 0.1K.

Results

The coupling efficiency is determined from this asymptotic power level and the calculated conduction heat flow. For targets with low coupling efficiency, there was insufficient incident laser power to melt the fuel when operating in the exchange gas conduction regime. Since we have not evaluated the heat flow in the molecular bombardment regime we did not determine absolute laser power coupling efficiencies for these targets. However, the relative heating efficiency of 488 nm and 632 nm wavelength illumination is determinable by comparing power levels at a particular pressure setting.

The bare glass target BF9 displayed low coupling for both 488 and 632 nm. Comparison of data taken with sample cell temperatures of 14.4K and 17.7K indicate that the He-Ne laser light (632 nm) is about 60-70% as effective in producing target heating in bare glass as the 488 nm Ar ion laser light. With a cell termperature of 14.4K and with 50 µm Hg of helium exchange gas the power incident required to melt the fuel is 2.15 mW and 1.55 mW for He-Ne and Ar ion illumination respectively. We estimate the coupling efficiency of 488nm light for this target to be less than 1.5%.

Coupling efficiencies for the CF and CH polymer coated targets were considerably larger than that obtained for the bare glass target. For target BF13 (20.74 µm of CH) data was obtained at 9.7K and 11.5K. With 2000 µm of exchange gas at 9.7K, the 488 nm laser power required to melt the fuel was 1.1 mW. When compared to the calculated heat flow of .145 mW, this gives a absolute coupling efficiency of 13.2%. With

200 µm of exchange gas we obtained 3.4 mW and 0.47 mW power levels for He-Ne and Ar ion laser light respectively giving a relative coupling efficiency of 13.8% and a derived absolute coupling efficiency for the He-Ne illumination of 1.8%. Similar results were obtained with a cell temperature of 11.1K with an absolute coupling efficiency for Ar ion illumination of 10.9% and a derived absolute coupling efficiency for He-Ne of 1.4%.

The behavior of the CF coated targets BF8 and BF14 was similar to that obtained for the CH targets with blue light heating efficiency being substantially higher than that obtained for red light. For target BF8 (15.5 µm CF) with a chamber temperature of 11.1K and exchange gas pressure of 2000 µm, .875 mW of 488 nm Ar ion power was required to melt the fill which when compared to the calculated heat flow of .160 mW gives an absolute coupling efficiency of 18.3%. Results obtained at 200 µm indicate power levels required to melt the fuel of 2.1 mW and .28 mW for 632 nm He-Ne and 488 nm Ar ion illumination respectively. We arrive at a derived absolute coupling efficiency for 632 nm illumination of 2.4%. With target BF14 at 9.9K and 11.05K 488 nm Ar ion coupling efficiency is 16.9% and 21.9% respectively. Derived coupling efficiency for 632 nm He-Ne illumination are 1.6% and 1.58% obtained at 9.9 and 11.05K respectively.

We believe the largest source of measurement error to be due to variability in the focusing and alignment of the heating laser beam with respect to the target. Small shifts in these parameters could act to alter the amount of target material present in the beam path. A secondary effect of off axis alignment is increased reflection loss for large angles of incidence between the target surface normal and the beam.

An implicit assumption in the analysis of this experiment is the uniformity of target temperature. With the nonuniform heating geometry employed one expects that some variation of steady state temperature across the target would be present. However the expected temperature range is thought to be small (less than .1K) and probably not significant. The sources of error listed could be largely rectified by utilizing a uniform intensity heating laser beam which would minimize the effects of beam misalignment. Implementation of these measures was precluded due to available laser power and sample cell optical access limitations.

Conclusions

The utility of laser beam heating of polymer coated and bare glass cryogenic ICF targets has been evaluated for light of 632 nm and 488 nm wavelengths. For all targets the coupling efficiency was higher for blue light than for red light, marginally so for bare glass and significantly so for polymer coated targets. This higher absorption efficiency for blue light, while appearing to be advantageous for LHPFR applications, may in fact create problems. The majority of the blue light absorption and heating will occur in the polymer layer with the strong possibility of damage being incurred due to thermal expansion. This may indicate a greater liklihood of target damage arising from ASE irradiation for driver lasers operating in the green or blue.

The technique described for measuring coupling efficiency may, with improvements cited, be applicable to accurately measuring optical absorption coefficients at cryogenic temperatures of weakly absorbing transparent materials. One could conceivably utilize data such as that presented in Figure 4b to investigate cryogenic thermal transport properties of gaseous helium for small scale lengths.

We wish to gratefully acknowledge Mr. Scott L. Bass, United States Military Academy who assisted in experimental setup and data taking.

REFERENCES

1. J. F. Miller, "A New Method for Producing Cryogenic Laser Fusion Targets," Adv. in Cryog. Eng. 23, K. D. Timmerhaus Ed.

2. S. Weber and G. Schmidt, Leiden Comm. No. 246C (1936)

FIGURE CAPTIONS

Fig. 1. Schematic of cryogenic sample cell.

Fig. 2. Schematic of optical system employed for heating and observing target.

Fig. 3. Geometry of heating laser fluence on spherical cryogenic target.

Fig. 4. (a) 488 nm Ar ion laser power incident on target BF14 required to melt DT fill as a function of helium exchange gas pressure for sample cell temperatures of 9.9K (■) and 11.65K (▲). (b) Pressure dependence of 632 nm He-Ne laser power required to melt fill in target BF14 at 9.9K (■) and 11.25K (▲).

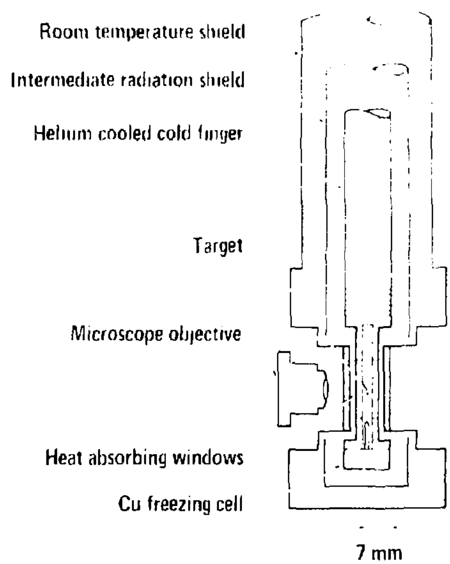
Room temperature shield
Intermediate radiation shield
Helium cooled cold finger
Target
Microscope objective
Heat absorbing windows
Cu freezing cell
7 mm

Figure 1

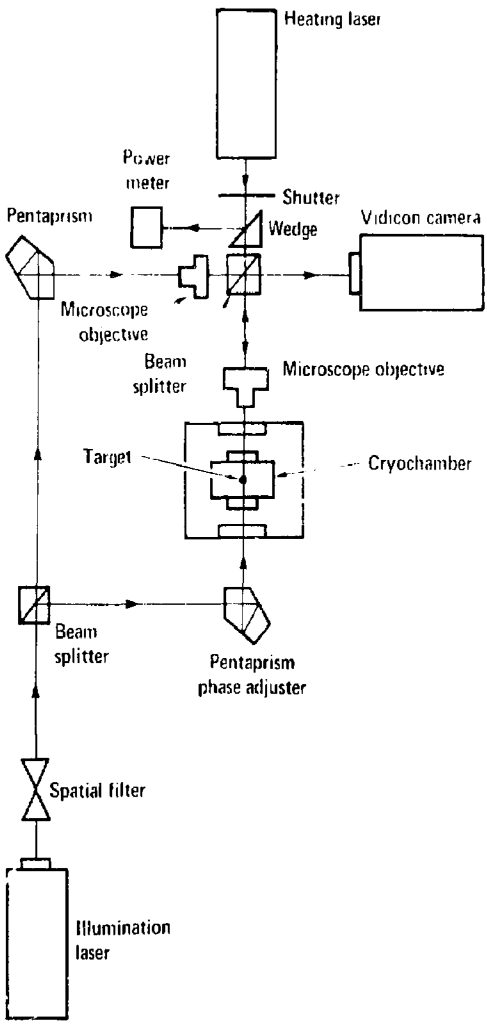

Heating laser
Power meter
Shutter
Pentaprism
Wedge
Vidicon camera
Microscope objective
Beam splitter
Microscope objective
Target
Cryochamber
Beam splitter
Pentaprism phase adjuster
Spatial filter
Illumination laser

Figure 2

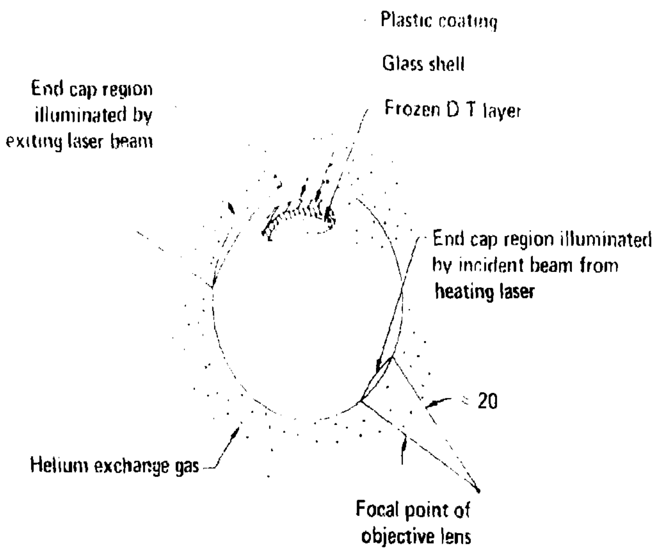
Plastic coating
Glass shell
Frozen D T layer
End cap region illuminated by exiting laser beam
End cap region illuminated by incident beam from heating laser
20
Helium exchange gas
Focal point of objective lens

Figure 3

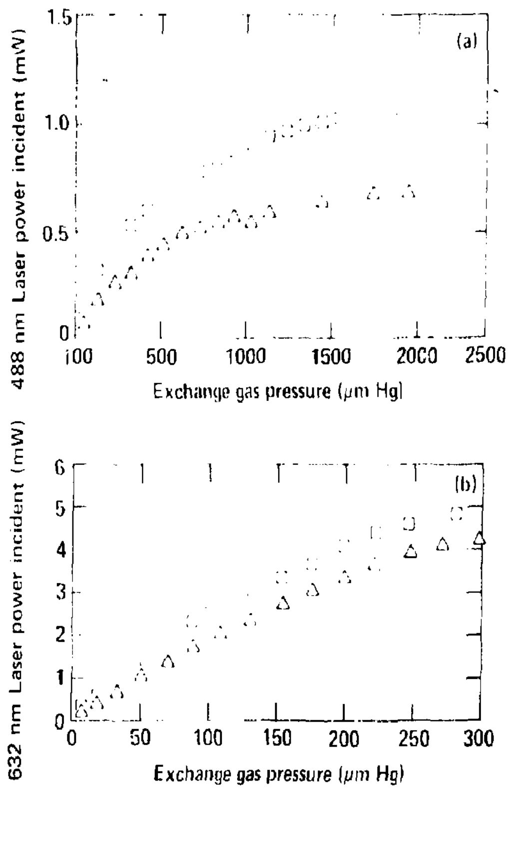

(a)
488 nm Laser power incident (mW)
Exchange gas pressure (μm Hg)
(b)
632 nm Laser power incident (mW)
Exchange gas pressure (μm Hg)

Figure 4